Journal of
Materials Chemistry B

Materials for biology and medicine

Accepted Manuscript

This article can be cited before page numbers have been issued, to do this please use: V. Guerrero-Florez, S. C. Mendez, A. A. Patron, V. Rodríguez González, D. Blach and F. Martínez O., *J. Mater. Chem. B*, 2020, DOI: 10.1039/D0TB00240B.

ROYAL SOCIETY OF CHEMISTRY

rsc.li/materials-b

View Article Online
DOI: 10.1039/D0TB00240B

Gold Nanoparticle-Mediated Generation of Reactive Oxygen Species During Plasmonic Photothermal Therapy: A Comparative Study for Different Particles Size, Shape, and Surface Conjugation

Valentina Guerrero-Florez, [a] *Stelia C. Mendéz-Sánchez,* [b] *Araceli Patrón-Soberano,* [c] *Vicente Rodríguez-Gonzáles,* [d] *Diana Blach,* [a] *Fernando Martínez O.* [a]*

[a] Centro de Investigaciones en Catálisis (CICAT), Escuela de química, Universidad Industrial de Santander, Km 2 vía El Refugio, Piedecuesta, Colombia.

[b] Grupo de Investigación en Bioquímica Y Microbiología (GIBIM), Escuela de química, Universidad Industrial de Santander, Bucaramanga, Colombia.

[c] División de Biología Molecular, Instituto Potosino de Investigación Científica y Tecnología, San Luis Potosí, S. L. P., México.

[d] División de Materiales Avanzados, Instituto Potosino de Investigación Científica y Tecnología, San Luis Potosí, S. L. P., México.

* Corresponding author.

Email: fmartine@uis.edu.co

Telephone: (+57) 7 – 6344000 ext. 1399

View Article Online
DOI: 10.1039/D0TB00240B

ABSTRACT

Gold nanoparticles (AuNPs)-mediated photothermal therapy represents an alternative to the effective ablation of cancer cells. However, the photothermal response of AuNPs must be tailored to improve the therapeutic efficacy of plasmonic photothermal therapy (PPT) and mitigate its side effects. This study presents an alternative to ease the tuning of photothermal efficiency and target selectivity. We use laser-treated spherical and anisotropic AuNPs with different sizes and biocompatible folic acid (FA)-conjugated AuNPs (FA-AuNPs) in the well-known human epithelial cervical cancer (HeLa) cell line. We show that large AuNPs produce a more significant photothermal heating effect than small ones. The thermal response of spherical AuNPs of 9 nm was found to reach a maximum increase of 3.0 ± 1 °C, whereas, with spherical AuNPs of 14 nm, the temperature increased by over 4.4 ± 1 °C. Anisotropic AuNPs of 15 nm reached a maximum of 4.0 ± 1 °C, whereas anisotropic AuNPs of 20 nm reached a significant increase of 5.3 ± 1 °C in the cell culture medium (MEM). Notably, anisotropic AuNPs of 20 nm successfully demonstrates the potential for use as a photothermal agent by showing reduced viability down to 60% at a concentration of 100 μM. Besides, we reveal that high concentrations of reactive oxygen species (ROS) are formed within the irradiated cells. It is likely to give rise in combination with stress by photothermal heating, resulting in significant cell death through acute necrosis by compromising the plasma membrane integrity. Cell death and ROS overproduction during PPT were characterized and quantified using transmission electron microscopy (TEM) and confocal fluorescence microscopy with different fluorescent markers. In addition, we show that FA-AuNPs induce cell death through apoptosis by internal damage, whereas diminishing ROS formation during PPT treatment. Our findings suggest the ability of plasmon-mediated ROS to sensitize cancer cells and make them vulnerable to photothermal damage, as well as the protective role of FA-AuNPs from excessive ROS formation, whereas reducing the risk of undesired side effects due to necrotic death pathway. It allows an improvement in the efficacy of AuNP-based photothermal therapy and a reduction in the number of exposures to high temperatures required to induce thermal stress.

Keywords: Folic acid, Gold nanoparticles, Laser irradiation, Photothermal effect, Reactive oxygen species.

View Article Online
DOI: 10.1039/D0TB00240B

INTRODUCTION

PPT for cancer treatment has emerged as a slightly invasive treatment to selectively target and kill cancer cells in which the photon energy is converted into thermal energy to induce irreversible cell damage [1], [2]. Developments of nanoparticles (NPs), which are capable of an efficient heat generation under illumination via laser radiation, and their use as photothermal agents have attracted considerable attention in recent years [3]. Nanotechnology has been explored news alternatives for localized heating using NPs with superior thermal properties [4]. Among them, AuNPs are outstanding photothermal agents for cancer therapy applications due to their strong optical properties. They exhibit efficient local heating after direct excitation of localized surface plasmon oscillations (LSPR), *i.e.*, light is strongly absorbed and then quickly converted to heat by a series of non-radiative processes. The strong absorption, efficient heat conversion, and inherent low toxicity make them especially attractive in therapeutic applications [5]. When AuNPs absorb electromagnetic energy, a non-radiative mechanism is carried out to dissipate the absorbed energy, inducing a rise in the temperature of the local environment; *viz.* the photothermal effect that can be used to promote the death of cancer cells [6]. Hence, the photothermal response of several gold nanostructures, including nanorods, nanoshells, nanoclusters, and nanocages, has been exploited for the destruction of cancer cells [7].

Beyond using gold nanomaterials as PPT agents, some studies have observed that reactive oxygen species (ROS) are formed when noble metal nanostructures are irradiated by employing either continuous-wave (CW) or pulsed laser [9], [10]. In particular, it was reported that spherical metal NPs, including Au, Ag, and Pt, can also yield chemical effects through the formation of ROS upon laser excitation [11], [12]. The exact mechanism leading to ROS production is poorly understood. However, it has been established that ROS can be produced in response to heat stress during PPT treatment [13]. ROS is known to play an essential role in the photodynamic therapy (PDT) where the activation of an organic photosensitizer by the light of an appropriate wavelength generates reactive oxygen species (ROS) in the form of free radicals or singlet oxygen [14]. These organic or organometallic dyes are prone to photoinduced degradation and enzymatic degradation, which becomes a drawback to PDT treatments and limits their biomedical applications [15]. To overcome these limitations, many researchers have developed strategies to combine several modalities simultaneously and to produce multifunctional nanostructures such as gold nanorod-photosensitizer complexes to achieve both PDT and PPT [16], [17]. Therefore, AuNPs are expected to be better ROS photosensitizers than conventional organic dyes due to its superior photostability and resistance to enzymatic degradation [18]. Nevertheless, the possibility of a single nanomaterial composite based on AuNPs with multifunctional therapeutic capabilities has not yet been studied. It prompts us to examine the possibility of using AuNPs as a potential photosensitizer. However, the effectiveness of AuNPs as therapeutic agents also strongly depends on their surface properties. In this sense, FA has attracted much attention and is one of the most common biomolecules used as a conjugating agent on the surface of NPs to target cancer cells. FA is a member of the vitamin B complex

View Article Online
DOI: 10.1039/D0TB00240B

and is required in several metabolic pathways because it assists biosynthesis of nucleic acids and amino acids, whereby plays a vital role in tissue growth. The vitamin is consumed in high quantities by proliferating cells [19]. Folate receptors (FRs) are frequently overexpressed in many of the human cancerous cells, perhaps enabling the malignant cell to compete successfully for the vitamin when supplies are limited, they are only minimally distributed in healthy tissue [20]. Accordingly, this feature makes it a promising agent for cancer treatment because incorporation biocompatible targeting ligands, photothermal agents can be utilized for the targeted photothermal treatment of certain types of cancer cells [21].

In this work, we investigated the applicability of AuNPs and FA-AuNPs as materials for an efficient PPT in cancer treatment. We demonstrated how the size and shape of AuNPs affect the photothermal response on HeLa cells straightforwardly. To this end, we previously synthesized several anisotropic and spherical AuNPs via CTAB reverse micelles using a procedure developed in our previous work with sizes from 9 to 20 nm as measured by TEM [22]. To achieve the temperature increments, the AuNPs concentration of 10 to 100 μM were exposed to a CW red laser of 638 nm and 1.56 W/cm^2 with treatment exposure of 5 min. Besides, we noticed the advantage of using FA-AuNPs for specific targeting and the improvement uptake by cancer cells through FR mediated endocytosis. To the best of our knowledge, this is the first work in the literature that explores the role of FA in the thermally and chemically induced cell death through the formation of ROS, during PPT treatment on in vitro destruction of HeLa cells. We compared the cellular responses caused by the photothermal effect of AuNPs and FA-AuNPs. Both NPs are expected to exert differently photothermal effects and cell death, which are still poorly understood. The impact of both NPs was evaluated in terms of cell viability, morphological changes, apoptosis induction, and the formation of ROS.

METHODS

Materials

Folic acid ($C_{19}H_{19}N_7O_6$), Muse® Annexin V and Dead Cell Kit were purchased from Merck, glutaraldehyde solution 50% ($C_{17}H_{16}N_8O_8$), formaldehyde solution 37% (HCHO), Hoechst 33342, crystal violet ($C_{25}H_{30}N_3Cl$), 2,7-dichlorofluorescein diacetate (DCFDA), sodium chloride (NaCl), potassium chloride (KCl), sodium phosphate dibasic (Na_2HPO_4), sodium citrate tribasic dihydrate ($HOC(COONa)(CH_2COONa)_2\ 2H_2O$), minimal eagle medium (MEM), trypsin, and antibiotic were purchased from Sigma–Aldrich. Fetal bovine serum (FBS) was purchased from Microgen. The water used throughout the experiment was purified with a Milli-Q system from Millipore.

AuNPs Synthesis and Conjugation

Spherical AuNPs of 9, 14 nm, and anisotropic AuNPs of 15, 20 nm stabilized with L-cysteine were synthesized via CTAB reverse micelles well-known as a "nanoreactors." The methodology used to manufacture AuNPs in reverse micelles was developed in a previous study [22]. All AuNPs solutions were purified by centrifugation for 20 min at 10000g and redispersed in

View Article Online
DOI: 10.1039/D0TB00240B

deionized water twice to remove CTAB excesses. The AuNPs were then conjugated with FA to increase their stability and biocompatibility. A 1×10-3 M aqueous solution of FA at pH 11 (1 M NaOH) was added to the solid obtained in the precipitation and phase transfer process. Then, FA-AuNPs solutions were vigorously stirred for 30 min at room temperature and subsequently centrifuged (10000 g, 20 min) to remove unbound FA molecules and dispersed in cells medium MEM. FA and FA-AuNPs solutions were analyzed by fluorescence spectroscopy with a Perkin Elmer's LS-55 spectrofluorometer by using an excitation wavelength of 364 nm. Measurements of Z-potential were carried out via a Zetasizer Nano's ZS90 equipment for each one of these solutions.

Photothermal Heating of AuNPs Solutions

The different AuNPs were diluted in cell culture media. AuNPs solutions were loaded into a standard quartz cuvette and then exposed using a ThorLabs' diode laser of 638 nm for increasing the irradiation times and the temperature measured by directly placing a thermocouple into solutions over 10 min of laser exposure. To ensure uniformity, the initial temperature of all solutions was 25 ± 1°C.

Cell Culture and Treatments with AuNPs

HeLa cell line was obtained from American Type Culture Collection (ATCC, USA)**.** Cells were maintained in Minimal Eagle Medium (MEM) supplemented with 7% v/v fetal bovine serum (FBS) and 1% v/v antibiotic under standard conditions at 37 °C and a humidified atmosphere containing 5% CO2 and 95% air. From growth to confluency, cells were trypsinized, counted by utilizing a hemocytometer, and cultured into a fresh medium. For the experiments, cells were seeded at a density of 1x104 cells/well on a 96-well plate in a volume of 200 µL containing EMEM supplemented medium at 37 °C, 5% of CO2, and an atmosphere of 95% air for 24 h. Upon 70% of confluence, cells were exposed to various concentrations of AuNPs and FA-AuNPs (10, 50, and 100 µM) for 4 h. For PPT studies, cells were grown with the same conditions described above. After overnight incubation, the growth media was replaced by varying concentrations of AuNPs and FA-AuNPs (*i.e.,* 10, 50, and 100 µM). After incubation for 4 h with AuNPs and FA-AuNPs and a subsequent replacement of the culture media (for removing free agents), cells in the culture chambers were exposed to 638 nm laser irradiation with a beam diameter of 5 mm at 600 mW and 1.56 W/cm^2 during 5 min. A medium supplemented with 7% FBS was used in all the experiments.

The uptake of FA-AuNPs was analysis also in the African green monkey kidney cell line (Vero) as a healthy cell. The cells were cultured in MEM supplemented with 7% v/v FBS and 1% v/v antibiotic. Cell cultures were maintained under standard conditions at 37 °C and a humidified atmosphere containing 5% CO2 and 95% air.

View Article Online
DOI: 10.1039/D0TB00240B

Crystal Violet Cell Viability Assays

The Crystal Violet staining (CVS) is a colorimetric assay based on the growth rate reduction from cell culture plates during cell death. This feature can be used to indirectly assess cell death and determine differences in proliferation rate [23]. CVS assay was employed to evaluate cell viability after treatment with AuNPs. After incubation of the cells with different types and concentrations of AuNPs, the supernatant was removed, and the cells were washed with PBS fixed with methanol for 10 min, stained with crystal violet 0.2% in ethanol 2% for 5 min, and washed 10 times with PBS. Cells were treated with sodium citrate in ethanol 50% for 10 min, and absorbance was measured at 550 nm using a Multiskan™ GO's microplate reader. The absorbance values obtained allow us to calculate the cell viability of treated cells versus control untreated cells.

Flow Cytometry Measurement

Flow cytometry was performed to differentiate apoptosis from necrotic cell death induced by laser-treated AuNPs and FA-AuNPs. Cells (5.0×10^5 cells per well in 12-well plates) were cultured in MEM supplemented with 7% FBS and incubated at 37 ºC and 5% CO2 for 24 h. AuNPs and FA-AuNPs laser-treated cells were harvested and washed twice in PBS and stained with Muse™ Annexin V and Dead Cell reagent as per manufacturer's instructions [24]. This assay employs Annexin V to detect phosphatidylserine (PS) on the external membrane of apoptotic cells. A dead cell marker (7-AAD) is also used as an indicator of cell membrane structural integrity. Flow cytometry was performed using Muse™ Cell. Data was collected for 10000 gated events using 488 nm light output from an Ar laser as an excitation source.

ROS Measurement

After PPT treatment, the ROS levels in cell culture media were determined by incubating HeLa cells with culture media containing AuNPs at 100 μM and exposing the samples to 638 nm laser as previously described. In this assay, cells were seeded in a black 96-well plate to avoid spectral interferences. Subsequently, the laser-treated media were removed, and cells were washed with PBS and incubated with 200 μL of DCFDA (50 μM). The solutions were incubated in the dark for 30 min at 37 °C with 5% CO_2. Then, the fluorescence of the oxidized DCF was measured by using an excitation wavelength of 485 nm and the emission of 525 nm during 4 h for each 10 min employing a Fluoroskan™ Microplate Fluorometer. Non-irradiated AuNPs and cells treated with a solution of H_2O_2 400 μM were used as a positive control.

Fluorescence Microscopic Images

HeLa cells were seeded on coverslips and incubated at 37 ° C with a 5% CO_2 atmosphere for 24 h. Then, they were incubated with different types and concentrations of AuNPs and PPT treatment. The cells were washed with PBS and fixed with 4% formaldehyde in PBS for 1 h at 4 °C. Next, the formaldehyde was removed, and cells were stained blue by using 1.3 mg/mL Hoechst 33343 (nucleic acid stain) for 20 min in the dark at room temperature followed by 3 PBS washes. The cell morphology was observed through a Zeiss upright microscope (Axio

View Article Online
DOI: 10.1039/D0TB00240B

Imager M2) and an AxioCam MRm camera with FireWire (1,4 MP). The image processing was carried out via the Carl Zeiss ZEN 2012 (blue edition) software.

Transmission Electron Microscopy (TEM) of HeLa Cells

The ultrastructure of cells after laser-treated AuNPs was evaluated via TEM. HeLa cells were seeded in Corning™ Transwell™ multiwell plate with polycarbonate membrane inserts and incubated at 37 ° C with a 5% CO_2 atmosphere for 24 h. Then, they were incubated with 100 μM AuNPs. After each experimental condition, the cells in the Transwell were processed as [25]. Briefly, 2.5% glutaraldehyde solution was added to the apical, then the basolateral chamber of Transwell filters and cell monolayers were fixed for 1 h. Sorensen's phosphate buffer was applied for 10 min to rinse off the fixative. 1% Osmium tetroxide was added to stain cell monolayers for 1 h. After the removal of OsO4, Sorensen's phosphate buffer was applied for washing for 10 min. Next, dehydration of cell monolayers was carried out with ethanol at different concentrations as follows: 30% ethanol on both sides of the filters for 10 min; 50% ethanol for 10 min; 70% ethanol for 10 min; 90% ethanol for 10 min; and finally, 100% ethanol for 20 min three times. Cell monolayers were pre-embedded with a mixture of epoxy resin (Spurr Low-Viscosity Embedding Kit) and ethanol (1:1 v/v) for 1 h, followed by 2 h embedding in full epoxy resin (100%) at 37 °C, with 250 mL on the top and 600 mL on the bottom. Later, epoxy resin was eradicated and replaced with fresh resin. Note that resin should be gently added to both the top and bottom space of the Transwell filters and enough used to submerge the Transwell as a whole. The Resin is then polymerized in an oven at 60 °C for 24 h. Small sections of each Transwell were made with a Dremel tool. Then, ultrathin sections of 70 nm were obtained using an ultramicrotome (RMC), positioned on FCF -100 Cu and contrasted with 2% uranyl acetate for 15 min and 2% lead citrate for 7 min. After brief washing, grids were air-dried. Finally, the samples were examined on a JEM-200 CX (JEOL) transmission electron microscope at 100 kV and equipped with a digital camera (SIA).

Statistical Analysis

Results are expressed as the average ± standard deviation of three independent experiments. Statistical significance was calculated using ANOVA and multiple comparison analysis averages (Tukey) calculator (GraphPad Software, Inc.). In addition, p-values less than 0.05 (*), 0.01 (**), and 0.001 (***) were considered to be statistically significant.

RESULTS AND DISCUSSION

Spherical and anisotropic AuNPs, each one of two different sizes (9 and 14 nm, 15 and 20 nm, respectively), synthesized via CTAB reverse micelles were chosen to be tested as candidate photothermal agents in the well-known HeLa cell line. The synthetic and characterization procedures of these AuNPs are detailed in our previous work, so we invite the reader to consult it for complementary information [22]. Furthermore, these AuNPs were conjugated with FA to evaluate their biocompatibility and target cancerous cells. For this purpose, the surface physicochemical properties of FA-AuNPs were characterized to carry out the in vitro assays.

View Article Online
DOI: 10.1039/D0TB00240B

The influence of the size, shape, and surface conjugation on cytotoxicity and photothermal effect of AuNPs to HeLa cells, were elucidated.

Spectral Characterization of FA-AuNPs

The surface charge of FA-conjugated AuNPs was followed by zeta potential (ζ) measurement. It is important to note that ζ measurements were done in aqueous media at a pH of 7.0. The results are summarized in Figure 1. It is observed an inversion of the positively charged surface of 9 and 14 nm spherical AuNPs (i.e., ζ + 29.9, 62.3 mV), after conjugation with FA (i.e., ζ – 18.0, 28.9 mV), respectively. For the case of 15 and 20 nm anisotropic AuNPs, it showed the same inversion of zeta potential values, from (ζ + 28.3, 30.4 mV) to (ζ – 15.0, 21.2 mV). This behavior can be explained based on the ionization process of FA. The acid dissociation constant (pKa) of FA that was determined by a capillary electrophoresis technique to acquire four pKa values (i.e., 2.38, 3.46, 4.98, and 8.08) as overall equilibrium constants. pK_1, pK_2, and pK_3 constant values are related to deprotonation sequences α-COOH, β-COOH, and NH_2, respectively. The pK_4 value of folic acid was assigned to the NH/CO fragment of the pteridine ring (cf. the inset in Figure 1) [26]. Accordingly, the deprotonated folic species started to form in acidic conditions (pH from 2 to 5.5) and wholly formed in neutral and alkaline conditions (pH from 5.5 to 9.5). Then, either carboxylic or amine groups of the anionic FA allowed the electrostatic association with the surface of AuNPs, leading to a reversal surface charge from positive values for AuNPs, to negative values, for FA-AuNPs. Nevertheless, surface-enhanced Raman scattering (SERS) spectra and density functional theory (DFT) calculations indicated that the interaction of FA with AuNPs occurred primarily through the nitrogen atoms from their pteridine ring [27]. Besides, it was shown that N–Au bonding interaction might be formed in this system [28]. Furthermore, this FA conjugation onto AuNPs preserves NPs negatively charged and provides colloidal stability [29].

View Article Online
DOI: 10.1039/D0TB00240B

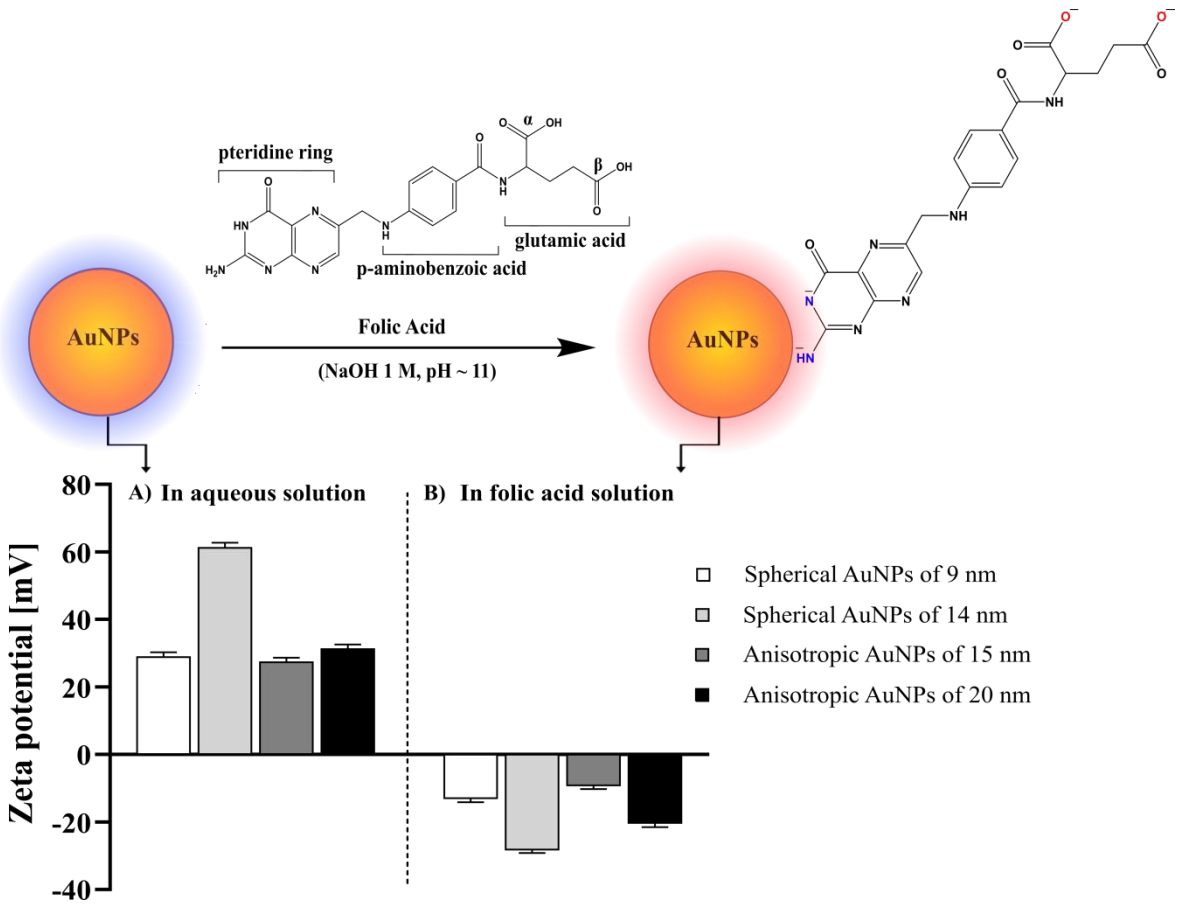

Figure 1. Zeta potential distribution of A) AuNPs and B) FA-AuNPs. Error bars represent standard error of mean with n = 3 per group. The inset shows a schema depicting the AuNPs conjugation using FA.

FTIR analysis was carried out to provide information about the functional groups involved in the conjugation process of FA to AuNPs. As Figure 2A shows, the bands that appear at 1688 cm^{-1} and 1602 cm^{-1} correspond to (-COO^-) symmetric stretch mode and (-NH) bending mode of FA, respectively. The shift from characteristic C=O stretching vibration of 1964 cm^{-1} to 1688 cm^{-1} belongs to the carboxyl change into the carboxylate group. Moreover, the bands between 1481 and 1451 cm^{-1} are attributed to the characteristic absorption band of the phenyl and pterin ring [30]. The characteristic IR absorption bands of FA are also observed in the spectrum of FA modified AuNPs. A simultaneous shift to a higher frequency is observed at a reduced intensity due to the small concentration of FA on the AuNP surface. These spectral differences from pure FA indicate structural changes in which -COO^- groups of the glutamic acid and -N-terminals groups of the pterin ring are involved in the interaction of FA with AuNPs.

View Article Online
DOI: 10.1039/D0TB00240B

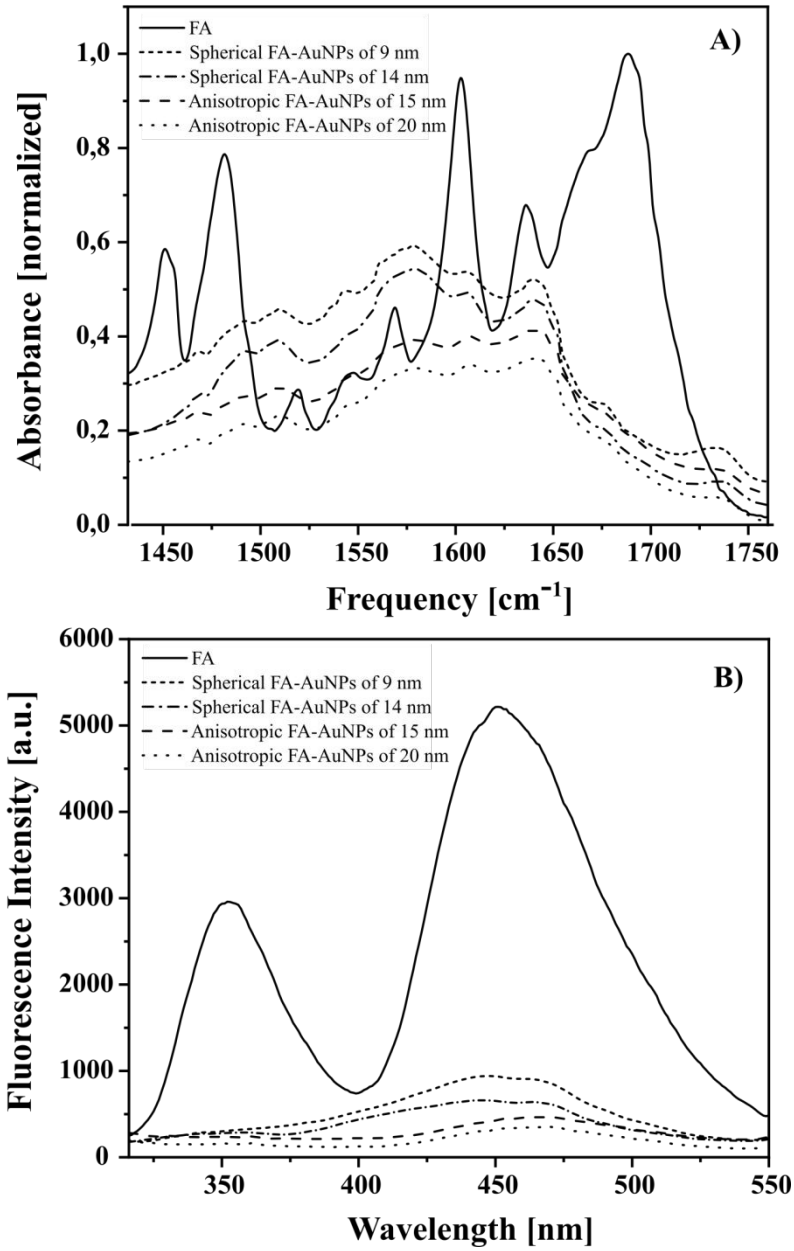

Figure 2. A) FTIR spectrum and B) fluorescence emission spectra of FA and FA-AuNPs at [Folic acid] = 1 × 10 $^{-3}$ M, [Au] = ~ 400 μM in water. The excitation wavelength used was 364 nm.

Theoretical calculations and as well as FTIR studies revealed that the coordination of terminal amine and carboxyl groups is based on a combination of electrostatic and hydrophobic interactions of the ligand and the NP surface, which are obtained by deprotonation of this donor groups [31]. Hydrophobic interactions are due to attraction between hydrophobic parts of the ligand and the metal surface that results in the formation of a non-covalent bond. Concomitantly, an ionic interaction is formed between negatively and positively charged groups and the surface of NP [32]. Molecular chromophores, as some biomolecules adsorbed on the surface of the NPs,

View Article Online
DOI: 10.1039/D0TB00240B

usually experience quenching of their fluorescence. Furthermore, the fluorescence background revealed that the AuNPs quenched excited states of the chromophores because they can also participate in an electron-transfer process and decrease the probability for radiative transitions [33], [34]. Therefore, fluorescence emission spectroscopy was performed to study the interaction of FA with AuNPs at the molecular level. Figure 2B shows the emission spectra of FA and FA-AuNPs suspended in water. The FA exhibit a two broad emission band: a weaker band centered around 352 nm and a stronger band centered around 451 nm.

In contrast, AuNPs-AF only presents a prominence of peak II over peak I at a reduced intensity. However, the fluorescence signals are significantly quenched by the AuNPs. It is important to note that a decrease in emission intensity is proportional to the reduction in the size of the AuNPs. These results are consistent with those previously reported by Paramanik *et al.* They found that quenching of fluorescence of the Safranine T dye decreased with the decrease in the size of the NPs of AgCl [35]. Aforesaid a behavior is related with successful conjugation of the FA to the AuNP surface due to only efficient quenching of fluorescence. This one is possible in the concentration range in which the available gold surface is not entirely saturated [36], Hence, it is possible to confirm that the FA concentration used was suitable to produce an efficient conjugation of FA to AuNPs.

Cytotoxicity Assay of AuNPs and FA-AuNPs

To evaluate the possible cytotoxic effects of AuNPs and FA-AuNPs, we used the crystal violet method in the presence of different concentrations of AuNPs. Crystal violet stain no-fragmented membrane cells, so it can be used as indicative of cellular viability [23]. Figure 3 shows the cytotoxicity of spherical and anisotropic AuNPs and FA-AuNPs on HeLa cells. The viability of non-conjugated spherical and anisotropic AuNPs treated cells were similar across different concentration. Overall, the viability of cells was not affected even at a high concentration of 100 μM. These data highlight that the cytotoxicity effect of AuNPs was not dependent on size or shape tested. Pan et al. reported similar results. They demonstrated the dependence of the toxicity of AuNPs with their size [37]. It was also showed that large AuNPs (10 or 16 nm) only penetrate through the cell membrane and are found only in the cytoplasm. In contrast, AuNPs between 2-6 nm successfully enters the cell nucleus, which results in higher cytotoxicity and immunological response [38], [39]. In this sense, our findings suggest that spherical and anisotropic AuNPs, with a size range of 9, 14, 15, and 20 nm, are not inherently toxic to HeLa cells at our test concentration.

View Article Online
DOI: 10.1039/D0TB00240B

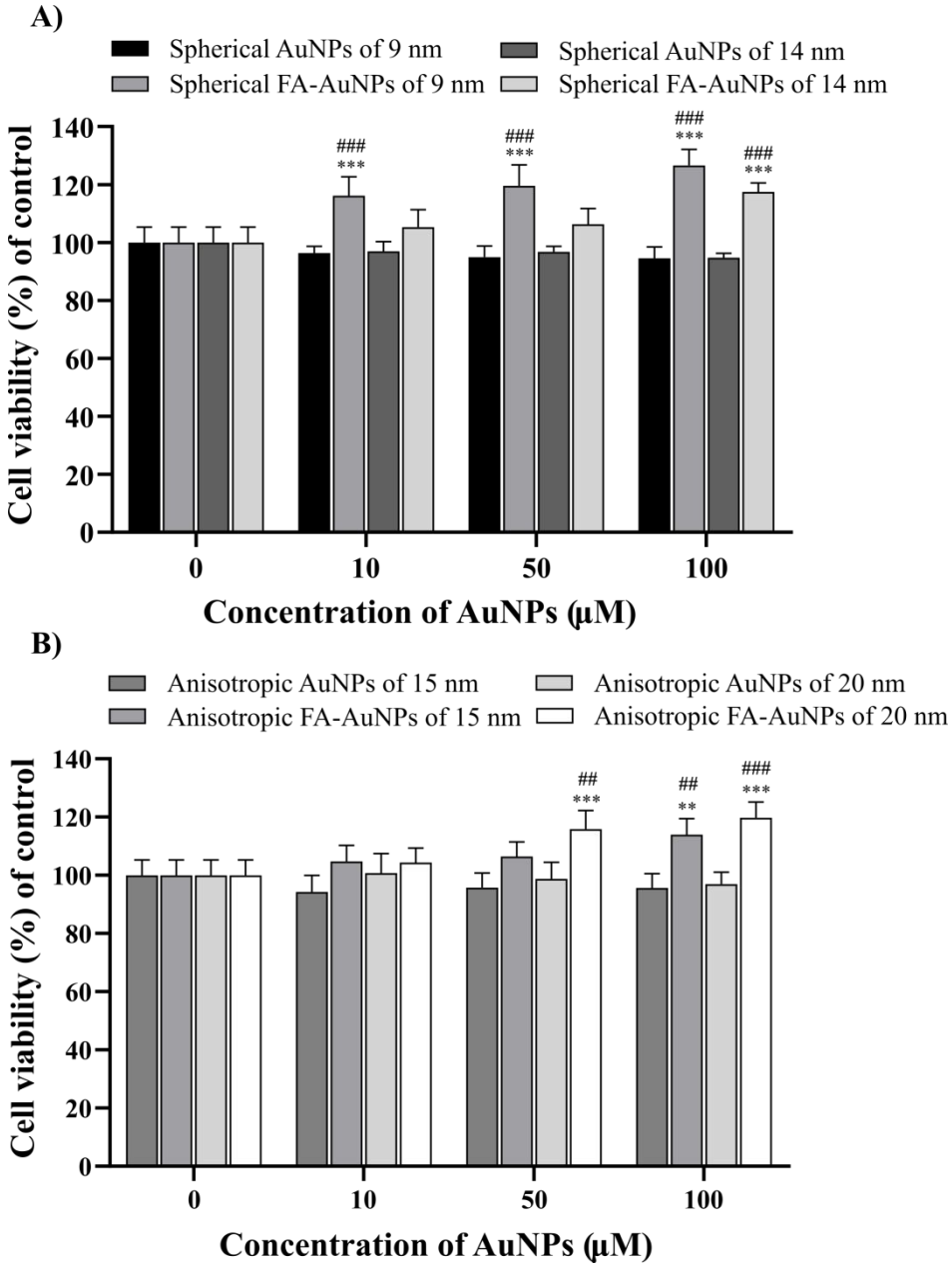

Figure 3. Cell viability assay of HeLa after exposure of various concentration of AuNPs and FA-AuNPs. The values represent the mean ± standard deviation of three independent experiments. *Significant difference to the control reference: *$p < 0.05$, **$p < 0.01$, ***$p < 0.001$ and #denote significant difference between AuNPs and FA-AuNPs: #$p < 0.05$, ##$p < 0.01$, ###$p < 0.001$.

On the other hand, when HeLa cells were incubated with spherical and anisotropic FA-AuNPs, the cell viability significant increased compared to control. At a concentration of 10 µM, cell viability increased to 116% in treatment with spherical FA-AuNPs of 9 nm. At 50 µM, the viability increased to 119% and 115% with spherical and anisotropic FA-AuNPs of 9 and 20 nm. Finally, at 100 µM, the viability increased to 126%, 117%, 113%, and 119% for treatments with spherical (of 9 and 14 nm) and anisotropic (of 15 and 20 nm) FA-AuNPs, respectively.

View Article Online
DOI: 10.1039/D0TB00240B

Considering that evaluated non-conjugated AuNPs do not acute cytotoxicity, these results suggest a strong activation of HeLa cells in which FA promotes cell proliferation. This behavior evidences the high biocompatibility of FA-AuNPs, as was previously observed [40]. Furthermore, the evidenced cellular response supposes an internalization via receptor-mediated endocytosis facilitated by the folate receptor (FR) overexpressed in HeLa Cells [41]. Additionally, comparing particle size with the same shape, a significant size-dependent effect is not noticed, whereas comparing anisotropic FA-AuNPs to spherical FA-AuNPs, an increase in viability is observed using the later. The internalization behavior can be significantly affected by the geometrical parameters as well as the uniform distribution of ligand molecules on the particle surface [42]. Therefore, spherical AuNPs with a very high aspect ratio favors FA-conjugation as was observed with ζ measurement.

PPT using spherical and anisotropic AuNPs

A diverse variety of AuNPs has been explored for use in therapy and imaging applications [43]. Key features to consider when selecting NPs for photothermal treatment are the wavelength of maximum absorption and the size of the particle [44]. In this section, the effect of AuNPs size and shape on the photothermal response in HeLa cells was conducted. The cells were incubated with 10, 50, 100 μM of AuNPs for 4 h and then irradiated with a laser of 638 nm at 600 mW for 5 min. Each sample was illuminated at a constant fluence rate of 1,56 W/cm^2. Light control experiments without AuNPs under 5 min light irradiation demonstrated that 96% of equivalent cells were viable, as shown in Figure S1 (cf. the supporting information file). Moreover, negligible differences in cytotoxicity were observed between light control experiments and control experiments, indicating that cells were not affected by the laser condition.

Figure 4 shows the cytotoxic effect of spherical AuNPs of 9 and 14 nm as well as anisotropic AuNPs of 15 and 20 nm after irradiation; it can be observed a concentration-dependent cell response across the sizes and shapes evaluated. At a high concentration of 100 μM, viability dropped to 82% using spherical AuNP of 9 nm, which is significantly lower than the viability of 65% obtained with spherical AuNPs of 14 nm. Likewise, at the same concentration, anisotropic AuNPs of 15 and 20 nm diminished cell viability significantly to 76% and 60%, respectively, compared to light control. Across the cellular response obtained in both cases, the most effective treatment was achieved using the large AuNPs, *i.e.,* treatment with spherical AuNPs of 14 and anisotropic AuNPs of 20 nm, suggesting a direct relationship between temperature and AuNPs size. The trend observed is consistent with the fact that the AuNPs directly absorb the laser light through the LSPR [45]. Spherical AuNPs of 14 nm shows a LSPR located at 563 nm, whereas the anisotropic AuNPs of 20 nm exhibit a broad absorption band centered at 656 nm that is overlapped by laser light wavelength of 638 nm (cf. Supplementary Figure S2 for details). This strong absorption of laser light directly induces temperature rises of the cells around the AuNPs and thus renders cell damage. The thermal response of the AuNPs solutions during laser irradiation was measured in the cell culture medium (MEM). As shown in Figure S3, the AuNPs suspensions exhibited a rapid size-dependent temperature increase. Upon increasing the exposure time to 10 min, the thermal response of spherical AuNPs of 9 nm was found to reach

View Article Online
DOI: 10.1039/D0TB00240B

a maximum increase of 3.0 ± 1 °C, whereas, with spherical AuNPs of 14 nm, the temperature increased by over 4.4 ± 1 °C. Anisotropic AuNPs of 15 nm reached a maximum of 4.0 ± 1 °C, whereas anisotropic AuNPs of 20 nm reached an increase of 5.3 ± 1 °C.

In comparison, the medium without AuNPs showed a minimal thermal response, only reaching an increment of ~ 1 °C. Nonetheless, among large spherical and anisotropic AuNPs, the later shows a higher photothermal efficiency indicating a substantial heating effect of AuNPs on cytotoxicity. All four AuNPs solutions displayed a strong thermal response, and the differences in temperature are again related to the overlap between the AuNPs LSPR and the wavelength of the laser source. When LSPR has shifted away from the laser wavelength, the extinction values, and, therefore, the light absorption at the laser wavelength becomes smaller, leading to the reduction in the photothermal conversion [46]. The enhanced thermal response of large anisotropic AuNPs, relative to the small spherical and anisotropic AuNPs, further demonstrating the size effect in photothermal heating [47] and suggests the potential of anisotropic AuNPs of 20 nm as active PPT agents.

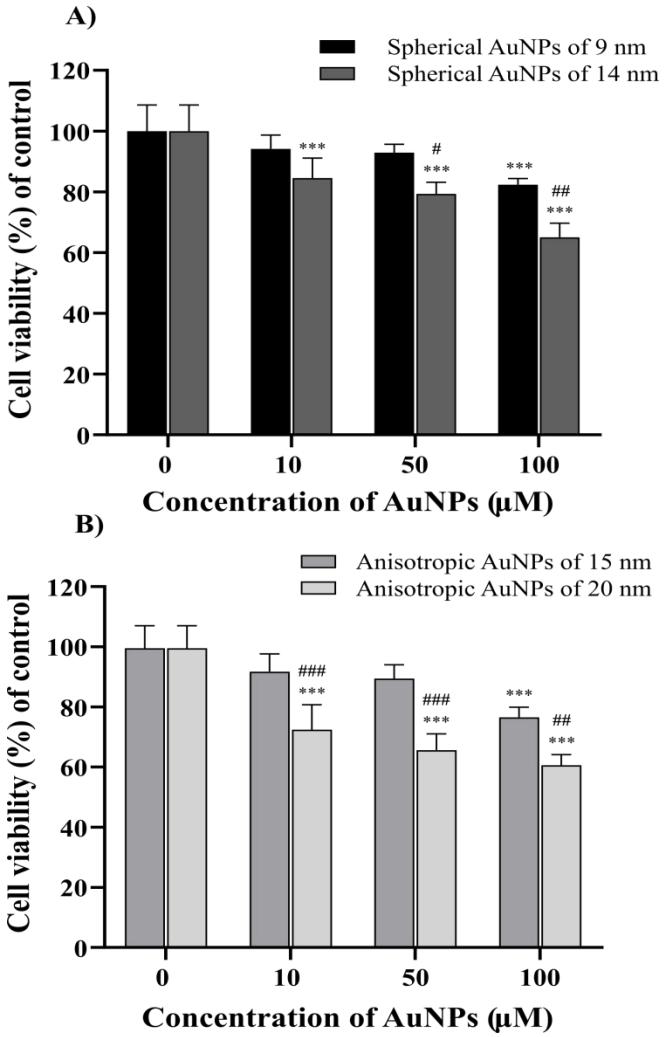

View Article Online
DOI: 10.1039/D0TB00240B

Figure 4. Cell viability assays of HeLa cells treated with spherical AuNPs of A) 9 nm and B) 14 nm; both exposed to 638 nm laser at 1.56 W/cm^2 power density for 5 min. The values represent the mean ± standard deviation of three independent experiments. *Significant difference to the control reference: $^{*}P < 0.05$, $^{**}P < 0.01$, $^{***}P < 0.001$ and $^{\#}$denote significant difference between the sizes of AuNPs: $^{\#}P < 0.05$, $^{\#\#}P < 0.01$, $^{\#\#\#}P < 0.001$.

The photothermal effect on the viability of HeLa cells was contrasted with cellular morphology changes evaluated through nuclear staining with Hoechst-33342 after irradiation. Changes in nuclear morphology serve to analyze cell death progression due to during apoptosis, the DNA becomes condensed. Still, this process does not occur during necrosis, where membranes integrity is involved [48]. Figure 5A shows the light control cells where polygonal morphology of HeLa cells and normal nucleus was observed under a fluorescence microscope. HeLa cells treated with 100 μM of spherical and anisotropic irradiated AuNPs resulted in significant nuclear morphology changes in response to treatment. Differential interference contrast microscopy showed that most of the HeLa cells became circular under the irradiated AuNPs-induced stress. Therefore, most of the cells lost the capacity of adhesion and progressively detached. The quantitative estimation of nuclear condensation and apoptotic bodies by image processing further confirmed the observation and allowed to compare the photothermal cell response with the different AuNPs evaluated (Figure 5B-C).

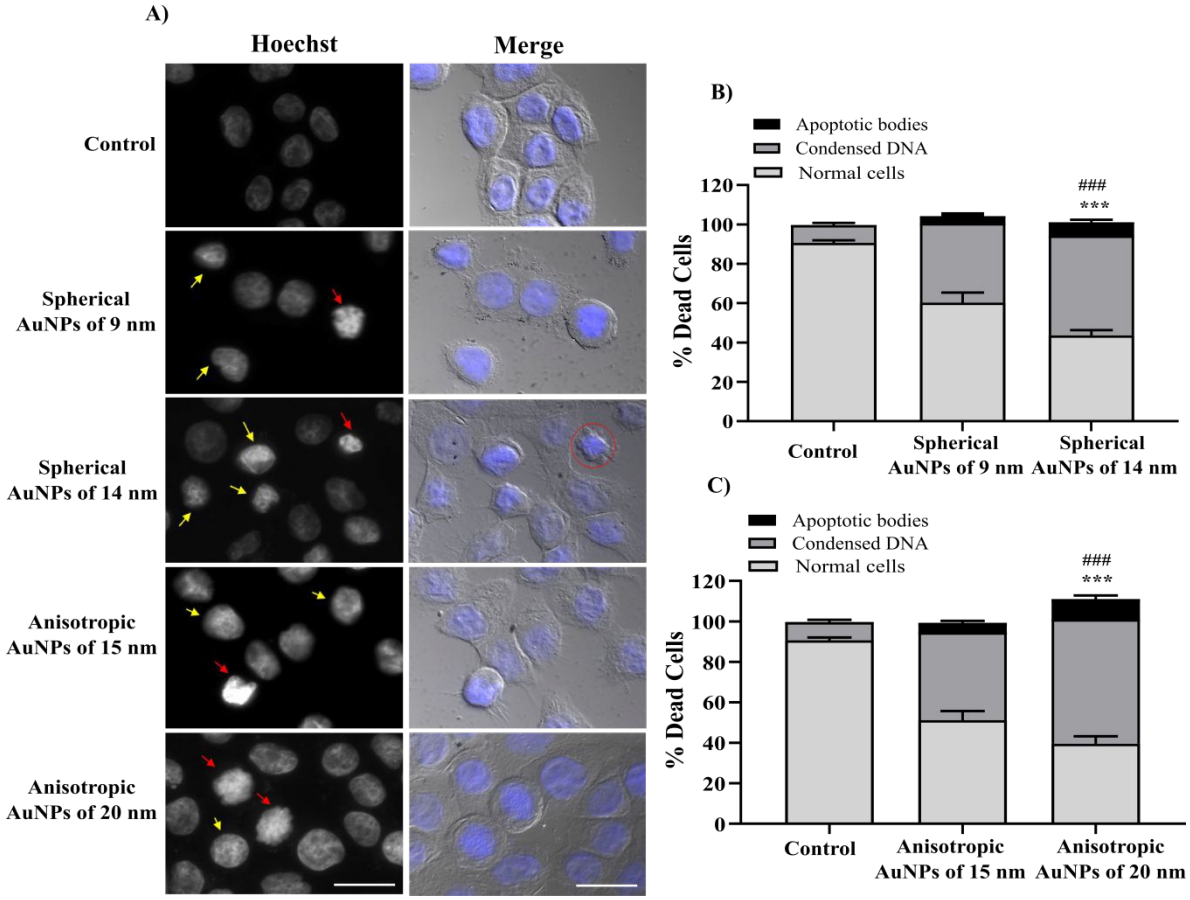

View Article Online
DOI: 10.1039/D0TB00240B

Figure 5. Nuclear staining of HeLa cells with Hoechst 33342: A) fluorescence images of HeLa treated with spherical AuNPs of 9 and 14 nm and anisotropic AuNPs of 15 and 20 nm at 100 μM. Hoechst 33342-stained nucleus HeLa cells demonstrate typical apoptotic morphology after 5 min of laser treatment with 638 nm at 1.56 W/cm^2: condensation of the nuclear material (yellow-arrow) followed by the formation of apoptotic bodies (red-arrows). Original magnification: ×100. Quantification of damaged cells of HeLa treated with B) spherical AuNPs of 9 and 14 nm. C) anisotropic AuNPs of 15 and 20 nm determined by image processing. The values represent the mean ± standard deviation of three independent experiments; ***denotes $P < 0.001$ with respect to the control; ###denotes $P < 0.001$ between the sizes of AuNPs. Bar = 11 μm

Again, the large spherical and anisotropic AuNPs are those that lead to more significant changes in nuclear morphology, a higher number of cells present altered morphology and the nucleus with the most condensed chromatin, even apoptotic bodies were found. 62% of HeLa cells treated with anisotropic AuNPs of 20 nm reveal significant alterations of the nucleus compared to the light control and spherical AuNPs of 14 nm. Interestingly, in Figure S4 is observed that at this concentration (100 μM) agglomerates of AuNPs decorated HeLa cells, suggesting a significant enhancement of the photothermal effects due to the collective heating effect [49], with a concomitant decrease in cell viability. The morphological analysis corroborated the observed trends in which cell death increases when the AuNPs concentration increases. *Huang et al.* also observed that aggregated gold nanospheres are responsible for the enhanced photothermal destruction of the human oral squamous carcinoma cell line (HSC 3) [50].

PPT compared between AuNPs and FA-AuNPs

Coherent with the insights obtained from the cellular response, significant attention was paid to the specific effects triggered by photothermal agents based on AuNPs conjugated with FA. In this study, it is expected that the FA-AuNPs could bind to FR on the HeLa cells surface and be selectively introduced to the target cells. As such, the photothermal effect on cell viability was evaluated under the same treatment conditions used for unconjugated nanoparticles (AuNPs) by the crystal violet method. In Figure 6, the comparison between the photothermal effect of AuNPs and FA-AuNPs on cell viability was revealed. It is important to note that a concentration-dependent response is not observed. Hereby, the viability of cells was significantly affected just with a concentration of 50 μM, which reduced the viability of all cell to 79% and 75% for the treatment with spherical FA-AuNPs of 9 nm and 14 nm, respectively. Likewise, at the same concentration, a reduction in cell viability of 66% and 61% was achieved for anisotropic FA-AuNPs of 15 and 20 nm, respectively. Increasing FA-AuNPs concentration from 50 to 100 μM did not reduce cell viability. Aforesaid cellular response was consistent across all types of FA-AuNPs. At a high concentration of 100 μM, the viability of HeLa cells treated with spherical FA-AuNPs of 9 and 14 nm dropped to 90% and 81%, respectively. Likewise, a reduction of cell viability of 87% and 74% were found in cell laser-treated with anisotropic FA-AuNPs of 15 and 20 nm, which in both cases was significantly lower than AuNPs.

When comparing AuNPs and FA-AuNPs, the cell viability decreased using spherical nanoparticles of 9 nm and anisotropic nanoparticles of 15 nm, both with 50 μM. On the other

View Article Online
DOI: 10.1039/D0TB00240B

hand, the viability increased using spherical nanoparticles of 100 nm and anisotropic nanoparticles of 20 nm. In all other treatments, no statistically significant differences were observed.

Considering that the ligands bind to the cells in a concentration-dependent manner and reached saturation for binding [51] suggests that the behavior observed may be essential for the regulated uptake of folates into cells in which the concentration that favors the interaction described above was 50 uM. Recently, Pinilla *et al.* also developed and compared photothermal agents based on AgNPs and FA-conjugated AgNPs on the HeLa cell line. The authors suggest that FA-AgNPs reduce up to 47% of the cell viability, using an 808 nm laser. This investigation conclusively revealed that FA-AgNPs are effective photothermal agents due to targeting the potential of FA on HeLa cells [52].

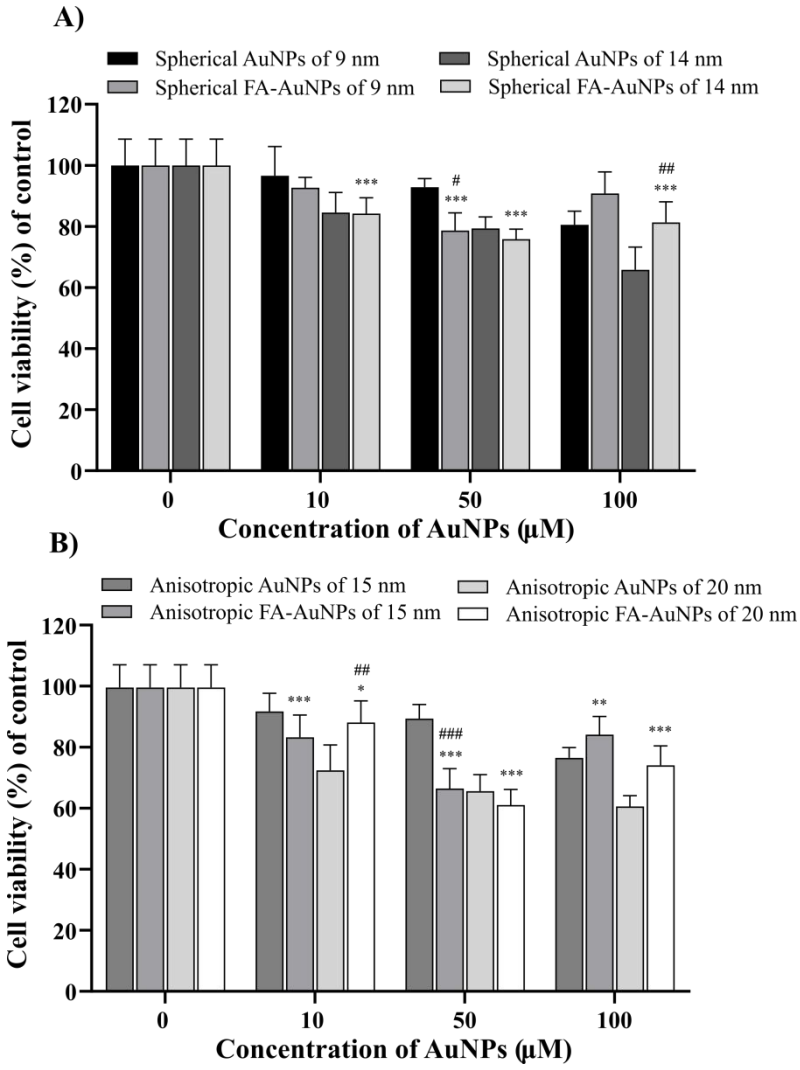

Figure 6. Cell viability assays of HeLa cells treated with various concentration of A) spherical AuNPs and B) anisotropic AuNPs; both exposed to 638 nm laser at 1.56 W/cm^2 power density for 5 min. The values represent the mean ± standard deviation of three independent

View Article Online
DOI: 10.1039/D0TB00240B

experiments. *Significant difference to the control reference: *$P < 0.05$, **$P < 0.01$, ***$P < 0.001$ and #denote significant difference between the sizes of AuNPs: #denote significant difference between AuNPs and FA-AuNPs: #p < 0.05, ##p < 0.01, ###p < 0.001.

To confirm AuNPs internalization and changes in cell morphology obtained from fluorescence microscopy data, we performed transmission electron microscopy (TEM) to image AuNPs in the cellular compartments and thoroughly analyze cell damage by its photothermal effect. Figure 7 shows that in all the cases, there is an intracellular uptake of AuNPs independently of its size, appearing in the form of aggregates according to electron-dense areas previously identified by TEM, as shown in Figure S5. This result indicates that AuNPs tend to be encapsulated inside subcellular organelles, similar to the endosomes and lysosomes morphology, containing numerous aggregate AuNPs. Ultrastructural examination show control HeLa cells with typical morphology, healthy mitochondria, intact cytoplasmic, and nuclear membrane (Figure 6I). In the case, treated HeLa cells (Figure 6A-H) showed a deterioration in mitochondria and cell organelles. Also observed loss of cell adhesion and decreased villi highlighting the loss of cell membranes integrity, which is severely affected by the photothermal effect because of AuNPs are inside the cells when irradiation occurs. Therefore, the intracellular surge in temperature strongly impacts cell membrane integrity [53]. The morphological changes observed in all treatments were a reduction in cell volume, cell shrinkage, and membrane blebs. Because the nuclei of these cells were pyknotic, and the plasma membrane integrity was also affected, all these findings strongly suggest that the morphological changes might be events ascribable of secondary or late apoptosis and necrosis. It is in agreement with morphological features of necrotic cells reported by Leonidova *et al.* [54], and Edinger and Thompson [55].

View Article Online
DOI: 10.1039/D0TB00240B

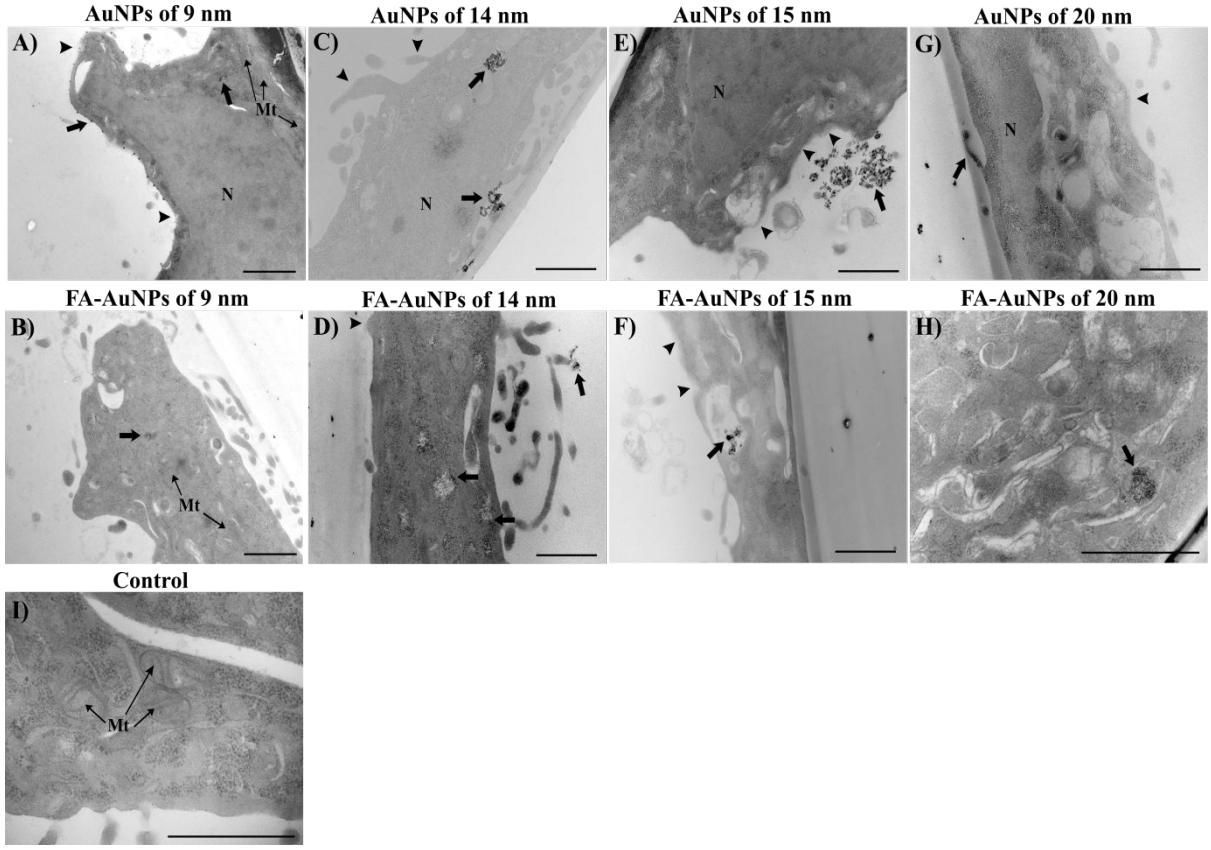

Figure 7. Transmission electron microscopy study of HeLa cell death morphology after 5 min of laser treatment at 638 nm and 1.56 W/cm^2 with 100 μM (A-D) spherical and (E-F) anisotropic AuNPs. A) AuNPs of 9 nm, B) FA-AuNPs of 9 nm, C) AuNPs of 14 nm, D) FA-AuNPs of 14 nm, E) AuNPs of 15 nm, F) FA-AuNPs of 15 nm, G) AuNPs of 20 nm, H) FA-AuNPs of 20 nm, I) HeLa control. Bar = 1 μm. NPs, Black flat arrow; N, Nucleus; Mt, Mitochondrion; arrowhead, cell membrane integrity loss.

To assess the extent of the uptake of FA-AuNPs into HeLa cells, we confirmed the differences in the uptake mechanism between AuNPs and FA-AuNPs by TEM images taken after the laser treatment, as shown in Figure 7B-H. Comparable to the uptake of AuNPs observed above, a higher number of FA-AuNPs are distributed in the cytoplasm; these FA-AuNPs appear to escape from the endosomes and entered the cytoplasm, suggesting that FA-AuNPs entered cells more efficiently as showed by more electron-dense areas. These results indicate that although AuNPs, as well as FA-AuNPs, are taken up by HeLa cells, the FA-AuNPs induce cellular uptake and different recognition from AuNPs. In some instances, confined within cytosolic vesicles, suggesting that FA-AuNPs are endocytosed, probably via receptor-mediated endocytosis. From the morphological changes that occur during HeLa cell death after laser-treated FA-AuNPs, large plasma membrane blebs were observed. These blebs were presented in different types of apoptotic cells [56]. Furthermore, the same treatment with FA-AuNPs in the Vero cell line was carried out to evaluate further if the cellular uptake of those FA-AuNPs is leading by FA-receptor-expressing, since their expressions are limited in healthy cells [57]. As can be seen in

View Article Online
DOI: 10.1039/D0TB00240B

Figure S6*,* Vero cells show deficient FA-AuNPs absorption, and the intracellular localization was less marked than with HeLa cells, indicating that the HeLa cellular greatly uptake of the particles is probably by the presence of FA.

To gain insight into the role of FA on cell death mediated by photothermal effect, we carried out a flow-cytometric assay to distinguish the mode of cell death upon exposure to activated AuNPs and FA-AuNPs after laser irradiation. Annexin V/7-amino-actinomycin (7-AAD) dyes were used to stain and exclude early apoptosis, late apoptosis, and necrosis. Annexin V successfully labels cells during early apoptosis, which binds to PS on the outer leaflet of the plasma membrane. Late apoptotic and necrotic cells lose their cell membrane integrity and are permeable to 7-AAD that selectively binds to GC regions of the DNA [58]. Therefore, stained cells were analyzed through the flow cytometer. The existence of four population distinguished from the following criteria: viable cells are annexin V and 7-AAD negative, early apoptotic cells are annexin V positive and 7-AAD negative, late-stage apoptotic and necrotic are annexin V and 7-AAD positive, and death cells (mostly nuclear debris) are annexin V negative and 7-AAD positive [24]. The percentage of populations were generated from dot plots and processed as a bar graph (Figure 8). As expected, treatment of HeLa cells with all types of AuNPs and FA-AuNPs result in the percentage of viable cells compared to our cell viability assay results using the same AuNPs concentration. It is essential to recognize that no differences were found in the mechanisms of cell death related to the size and shape of AuNPs tested. It makes sense because the phenomenon that is sought to mediate cell death is the photothermal effect of AuNP, so changes in the amount of cell death are expected due to its photothermal efficiency and no differences in the pathway of cell death.

View Article Online
DOI: 10.1039/D0TB00240B

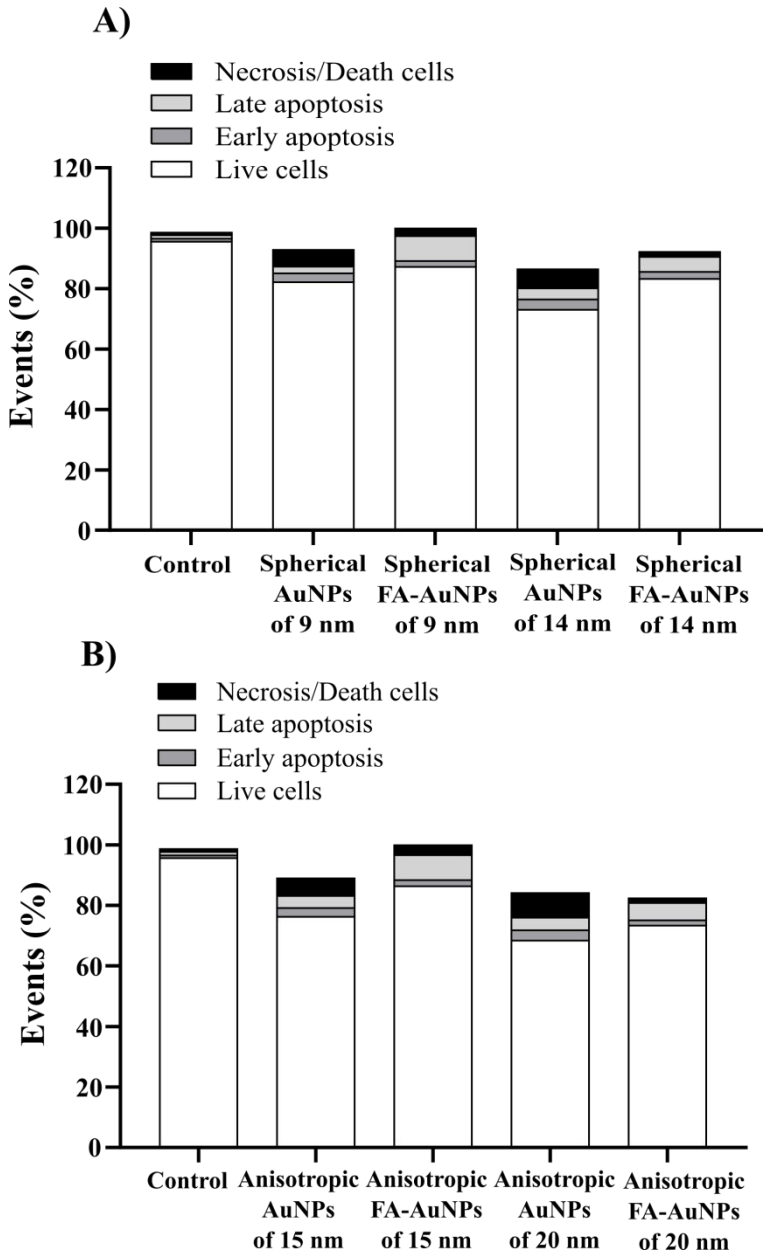

Figure 8. Annexin V and 7-AAD staining of HeLa treated with different AuNPs and FA-AuNPs solution at 100 μM for 4 h and exposed to 638 nm laser at 1.56 W/cm^2 power density for 5 min. Bar graph showing the rates of apoptosis and necrosis HeLa cell in individual groups. Cells stained with 7-AAD alone are necrotic, whereas cells stained with Annexin V alone represent early apoptosis. Cells at the final stage of apoptosis take up both stains.

Interestedly, the response of HeLa cells to FA-AuNPs was thoroughly different from AuNPs. Treatment with spherical FA-AuNPs of 9 and 14 nm caused the cells entering in late apoptosis increased by 5% and 8%, respectively. With the same non-conjugated AuNPs, the cells were found in the late apoptosis population to eventually undergo a majority death cell, where the plasma membrane lost its integrity. Then cell fragmented into nuclear debris forms in the

View Article Online
DOI: 10.1039/D0TB00240B

necrosis process [59], cells become permeable for 7-AAD either immediately or shortly before through early apoptosis. Therefore, these results suggest that cells are, in fact traversing through late apoptosis/necrosis as a result of cell died via necrosis but not through the apoptotic pathway. It is widely known that cell death triggered by PPT mainly induces necrosis, which is characterized by loss of plasma membrane integrity and the release of intracellular contents into surrounding tissues leading to detrimental inflammatory and immunogenic responses [60], which reduces the treatment efficiency.

Conversely, an indicator of either increased transition of early apoptotic cells to late apoptosis/necrosis was not observed with FA- AuNPs treatment, cells appear in the late stages of apoptosis or dead. In the same way, treatment with anisotropic FA-AuNPs of 15 and 20 nm, the percentage of late apoptosis was higher than the anisotropic AuNPs, in which the most considerable population was found in the final stage of cell death. These results show that HeLa cells are, in fact traversing through early apoptosis before reaching late apoptosis/necrosis, which further confirms that laser-treated FA-AuNPs induced cell death by an apoptotic mechanism. Therefore, it is noticeable that the mechanism of uptake of FA-AuNPs and, therefore, it is subsequent processing by HeLa cells, as well as its photothermal effect, could be different from AuNPs.

Previous reports established that ROS could be produced in response to heat stress during PPT with different NPs and mediate cell death in various cancer cells [17], [61], [62]. We were interested in probing if ROS would be generated in HeLa cells treated with AuNPs and FA-AuNPs before and after laser exposure. Therefore, the production of ROS during PPT treatment with spherical AuNPs and FA-AuNPs of 14 nm was investigated using a fluorescent 2,7-dichlorofluorescein (DCF) assay to measure the reactive oxygen levels in cell culture media before and after laser exposure. The treatment was performed using spherical AuNPs of 14 nm because induced slightly higher cell death than the smallest tested. As shown in Figure 9, the incubation of HeLa cells with AuNPs and FA-AuNPs alter the amount of endogenous ROS present in control in a dependent manner on the AuNPs conjugation before laser exposure. Notably, incubation with AuNPs led to a significant incremented in ROS levels compared to the untreated control, the amount of ROS present in FA-AuNPs containing cell media was negligible. However, cell viability tests did not show intrinsic cytotoxicity for any AuNPs. Therefore, the exposure to AuNPs themselves is not necessarily detrimental to cellular function as endogenous ROS exert an essential role in "redox" signaling pathways that contribute to healthy cell function [63]. After laser exposure, the amount of ROS in culture media containing AuNPs displayed a highly significant increase in fluorescence, confirming the formation of ROS during PPT treatment. It is important to note that the increment of the ROS levels is again higher than observed with FA-AuNP. Control without AuNPs or FA-AuNPs did not show any significant changes in fluorescence after laser exposure, indicating that the ROS formed during PPT treatment was produced by AuNPs. Accordingly, non-conjugated AuNPs displayed the most robust thermal response to PPT, besides the significant amounts of ROS produced during the treatment, resulting in cell death through oxidative damage, in addition to the toxicity

View Article Online
DOI: 10.1039/D0TB00240B

induced by photothermal heating. Comparable heat stress-induced ROS production, and accordingly, cell death would be expected with laser-treated FA-AuNPs. However, FA-AuNPs displayed the weakest thermal response to PPT treatment, and they also reduced any ROS produced during the treatment before oxidative damage could occur. The lack of cell death from the FA-AuNPs-treated samples further confirms the beneficial protective effect of ROS by the FA shell. The presence of FA reduces any ROS produced during treatment and even before laser exposure, making ineffectively the sensitize cancer cell to make them highly vulnerable to subsequent photothermal heating, resulting in observed marginal efficiency.

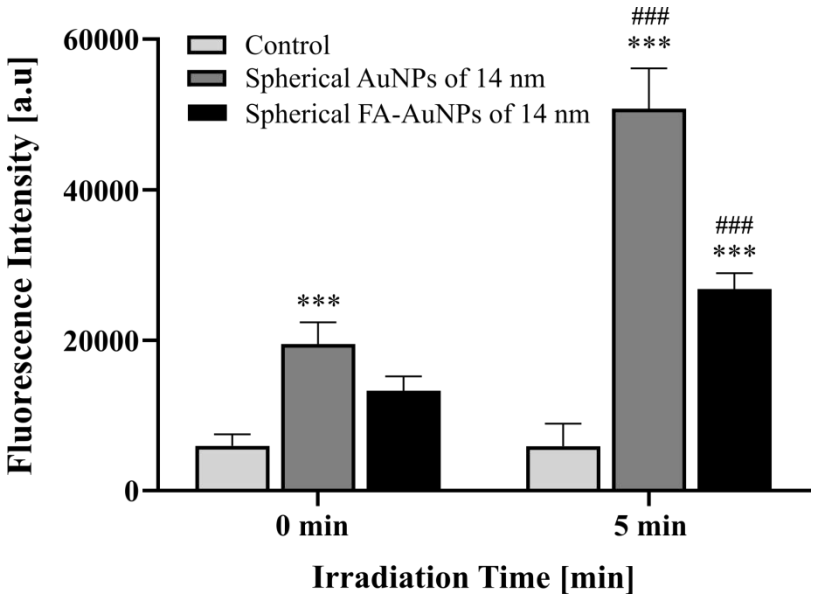

Figure 9. Quantitative measurements of ROS generation in cell media before and after 5 min of photothermal heating. The values represent the mean ± standard deviation of three independent experiments; ***denotes $P < 0.001$ with respect to the control; ###denotes $P < 0.001$ between laser-treated AuNPs and non-irradiated treated-AuNPs.

These results are in agreement with the derivatives in flow cytometry assay, as non-conjugated AuNPs after laser exhibit high production of ROS, which can increase the regulation of caspase protein to initiate cell apoptosis as observed [64]. Although the apoptosis and necrosis are not necessarily mutually exclusive, as demonstrated by high oxidative stress, where mixed death phenotypes have been observed [65]. Our findings confirm that laser-treated FA-AuNPs induced apoptosis rather than necrosis reduced concerns regarding side effects caused by the inflammatory cellular response in necrosis pathway [66]. These results indicate that AuNPs, as well as, FA-AuNPs can be employed not only as a source of heat but also as photosensitizers mediating generation of ROS under irradiation. The production of ROS is likely to produce a synergistic effect in combination with photothermal heating that results in effective cell death, further supporting the conclusion that ROS plays a significant role during PPT treatment. In

View Article Online
DOI: 10.1039/D0TB00240B

contrast, FA-AuNPs triggered synergistic effects between induces cell death by apoptosis while reducing the risk of undesirable side effects due to heat stress-induced ROS production.

CONCLUSIONS

The current work demonstrates that the photothermal properties of AuNPs can be modulated through variation of the size, shape, and surface conjugation to induce efficient cell death in PPT. Here, we showed that large spherical and anisotropic AuNPs exhibited significantly enhanced photothermal effects when irradiated with a red laser in comparison to the smallest AuNPs tested. At 100 μM, the viability of HeLa cells dropped significantly to 65% and 60% after laser-treated with spherical and anisotropic AuNPs of 14 and 20 nm, respectively. PPT treatment of the AuNPs results in cell death through acute necrosis by compromising the plasma membrane integrity and the formation of ROS, which is likely to give rise in combination with stress by photothermal heating. These AuNPs were used to demonstrate the targeted photothermal treatment after the incorporation of FA-conjugated AuNPs. The observed viabilities were 75% and 61% at 50 μM in the cases for FA-AuNPs of 14 and 20 nm, respectively. It is advantageous because lower concentrations of FA-AuNPs are required to achieve efficient cell death. FA-AuNPs are promising photothermal agents to PPT as led to apoptosis by internal damage, whereas diminished ROS produced during treatment. It conferred an additional advantage due to promote protective stress pathways preventing unwanted death as a result of heat-stress-induced ROS formation. More broadly, our findings exhibit a promising approach to achieving cancer cells die, which, based on TEM microstructural examination and ROS measurement during photothermal treatment, are ascribed to the sensitization effect arising from plasmon-mediated ROS, which plays a crucial role in enhancing the PPT efficacy.

ACKNOWLEDGEMENTS

We gratefully acknowledge the financial support for this study by the Universidad Industrial de Santander–UIS (Project DIEF 2303). The authors want to thank LINAN-IPICYT for the TEM sample characterizations.

CONFLICT OF INTEREST

The authors declare that they have no conflicts of interest to reveal.

REFERENCES

[1] E. B. Dickerson *et al.*, "Gold nanorod assisted near-infrared plasmonic photothermal therapy (PPTT) of squamous cell carcinoma in mice," *Cancer Lett.*, vol. 269, no. 1, pp. 57–66, 2008.

[2] X. Huang, I. H. El-Sayed, W. Qian, and M. A. El-Sayed, "Cancer cell imaging and photothermal therapy in the near-infrared region by using gold nanorods," *J. Am. Chem. Soc.*, vol. 128, no. 6, pp. 2115–2120, 2006.

[3] D. Pissuwan, S. M. Valenzuela, and M. B. Cortie, "Therapeutic possibilities of plasmonically heated gold nanoparticles," *Trends Biotechnol.*, vol. 24, no. 2, pp. 62–67, 2006.

View Article Online
DOI: 10.1039/D0TB00240B

[4] D. Jaque *et al.*, "Nanoparticles for photothermal therapies.," *Nanoscale*, vol. 6, no. 16, pp. 9494–530, 2014.

[5] S. Eustis and M. A. El-Sayed, "Why gold nanoparticles are more precious than pretty gold: Noble metal surface plasmon resonance and its enhancement of the radiative and nonradiative properties of nanocrystals of different shapes," *Chem. Soc. Rev.*, vol. 35, no. 3, pp. 209–217, 2006.

[6] J. H. Hodak, A. Henglein, and G. V Hartland, "Photophysics of Nanometer Sized Metal Particles : Electron-Phonon Coupling and," *J. Phys. Chem. B*, vol. 104, no. 43, pp. 9954–9965, 2000.

[7] J. Song, S. Kim, H. Doh, S. Jung, J. Nam, and S. Hwang, "Gold nanoparticle-mediated photothermal therapy: current status and future perspective," *Nanomedicine*, vol. 9, no. 13, pp. 2003–2022, 2014.

[8] J. T. Beckham *et al.*, "Microarray analysis of cellular thermotolerance," *Lasers Surg. Med.*, vol. 42, no. 10, pp. 752–765, 2010.

[9] G. Pasparakis, "Light-induced generation of singlet oxygen by naked gold nanoparticles and its implications to cancer cell phototherapy," *Small*, vol. 9, no. 24, pp. 4130–4134, 2013.

[10] D. Yoo *et al.*, "Double-effector nanoparticles: A synergistic approach to apoptotic hyperthermia," *Angew. Chemie - Int. Ed.*, vol. 51, no. 50, pp. 12482–12485, 2012.

[11] R. Vankayala, A. Sagadevan, P. Vijayaraghavan, C. L. Kuo, and K. C. Hwang, "Metal nanoparticles sensitize the formation of singlet oxygen," *Angew. Chemie - Int. Ed.*, vol. 50, no. 45, pp. 10640–10644, 2011.

[12] Ž. Krpetić, P. Nativo, V. Sée, I. A. Prior, M. Brust, and M. Volk, "Inflicting controlled nonthermal damage to subcellular structures by laser-activated gold nanoparticles," *Nano Lett.*, vol. 10, no. 11, pp. 4549–4554, 2010.

[13] M. Aioub, S. R. Panikkanvalappil, and M. A. El-Sayed, "Platinum-Coated Gold Nanorods: Efficient Reactive Oxygen Scavengers That Prevent Oxidative Damage toward Healthy, Untreated Cells during Plasmonic Photothermal Therapy," *ACS Nano*, vol. 11, no. 1, pp. 579–586, 2017.

[14] J. P. Celli *et al.*, "Imaging and Photodynamic Therapy: Mechanisms, Monitoring, and Optimization," *Chem. Rev.*, vol. 110, no. 5, pp. 2795–2838, May 2010.

[15] R. Batchelor, "Photodynamic therapy for the treatment of morphoea," *Clin. Exp. Dermatol.*, vol. 33, no. 5, pp. 661–663, 2008.

[16] B. Jang, J. Park, C. Tung, I. Kim, and Y. Choi, "Gold Nanorod - Photosensitizer," no. 2, pp. 1086–1094, 2011.

[17] W. S. Kuo *et al.*, "Gold nanomaterials conjugated with indocyanine green for dual-modality photodynamic and photothermal therapy," *Biomaterials*, vol. 33, no. 11, pp. 3270–3278, 2012.

[18] R. Vankayala, C. L. Kuo, A. Sagadevan, P. H. Chen, C. S. Chiang, and K. C. Hwang,

View Article Online
DOI: 10.1039/D0TB00240B

"Morphology dependent photosensitization and formation of singlet oxygen ($^1\Delta$<inf>g</inf>) by gold and silver nanoparticles and its application in cancer treatment," *J. Mater. Chem. B*, vol. 1, no. 35, pp. 4379–4387, 2013.

[19] A. C. Antony, "The Biological Chemistry of Folate Receptors HE ESSENTIAL role of intracellular folates in ef," vol. 79, no. 11, pp. 2807–2820, 1992.

[20] C. S. Kue, A. Kamkaew, K. Burgess, L. V. Kiew, L. Y. Chung, and H. B. Lee, "Small Molecules for Active Targeting in Cancer," *Med. Res. Rev.*, vol. 36, no. 3, pp. 494–575, Apr. 2016.

[21] S. Wang *et al.*, "Photothermal effects of supramolecularly assembled gold nanoparticles for the targeted treatment of cancer cells," *Angew. Chemie - Int. Ed.*, vol. 49, no. 22, pp. 3777–3781, 2010.

[22] V. Guerrero-Florez, D. Blach, and F. Martínez O, "Nonpolar Interface Composition in Cetyltrimethylammonium Bromide Reverse Micellar Environments to Control Size and Induce Anisotropy on Gold Nanoparticles," *ChemistrySelect*, vol. 4, no. 47, pp. 13983–13991, Dec. 2019.

[23] M. Feoktistova, P. Geserick, and M. Leverkus, "Crystal violet assay for determining viability of cultured cells," *Cold Spring Harb. Protoc.*, vol. 2016, no. 4, pp. 343–346, 2016.

[24] Q. R. Card, "Muse™ Annexin V & Dead Cell Kit User's Guide," vol. 100105, no. 4700, pp. 100105–100106.

[25] D. Ye, K. A. Dawson, and I. Lynch, "A TEM protocol for quality assurance of in vitro cellular barrier models and its application to the assessment of nanoparticle transport mechanisms across barriers," *Analyst*, vol. 140, no. 1, pp. 83–97, 2015.

[26] Z. Szakács and B. Noszál, "Determination of dissociation constants of folic acid, methotrexate, and other photolabile pteridines by pressure-assisted capillary electrophoresis," *Electrophoresis*, vol. 27, no. 17, pp. 3399–3409, 2006.

[27] J. J. Castillo, T. Rindzevicius, C. E. Rozo, and A. Boisen, "Adsorption and vibrational study of folic acid on gold nanopillar structures using surface-enhanced raman scattering spectroscopy," *Nanomater. Nanotechnol.*, vol. 5, no. 1, 2015.

[28] R. Di Felice and A. Selloni, "Adsorption modes of cysteine on Au(111): Thiolate, amino-thiolate, disulfide," *J. Chem. Phys.*, vol. 120, no. 10, pp. 4906–4914, 2004.

[29] X. Huang, P. K. Jain, I. H. El-Sayed, and M. A. El-Sayed, "Plasmonic photothermal therapy (PPTT) using gold nanoparticles.," *Lasers Med. Sci.*, vol. 23, no. 3, pp. 217–28, 2008.

[30] J. Zhang, S. Rana, R. S. Srivastava, and R. D. K. Misra, "On the chemical synthesis and drug delivery response of folate receptor-activated, polyethylene glycol-functionalized magnetite nanoparticles," *Acta Biomater.*, vol. 4, no. 1, pp. 40–48, 2008.

[31] M. A. Neouze and U. Schubert, "Surface modification and functionalization of metal and metal oxide nanoparticles by organic ligands," *Monatshefte fur Chemie*, vol. 139, no. 3, pp. 183–195, 2008.

View Article Online
DOI: 10.1039/D0TB00240B

[32] R. G. Rayavarapu, W. Petersen, C. Ungureanu, J. N. Post, T. G. Van Leeuwen, and S. Manohar, "Synthesis and bioconjugation of gold nanoparticles as potential molecular probes for light-based imaging techniques," *Int. J. Biomed. Imaging*, vol. 2007, 2007.

[33] G. Schneider, G. Decher, N. Nerambourg, R. Praho, M. H. V. Werts, and M. Blanchard-Desce, "Distance-dependent fluorescence quenching on gold nanoparticles ensheathed with layer-by-layer assembled polyelectrolytes," *Nano Lett.*, vol. 6, no. 3, pp. 530–536, 2006.

[34] B. I. Ipe, K. George Thomas, S. Barazzouk, S. Hotchandani, and P. V. Kamat, "Photoinduced charge separation in a fluorophore - Gold nanoassembly," *J. Phys. Chem. B*, vol. 106, no. 1, pp. 18–21, 2002.

[35] S. Pramanik, S. C. Bhattacharya, and T. Imae, "Fluorescence quenching of 3,7-diamino-2,8-dimethyl-5-phenyl phenazinium chloride by AgCl and Ag nanoparticles," *J. Lumin.*, vol. 126, no. 1, pp. 155–159, 2007.

[36] M. Montalti, L. Prodi, N. Zaccheroni, and G. Battistini, "Modulation of the photophysical properties of gold nanoparticles by accurate control of the surface coverage," *Langmuir*, vol. 20, no. 18, pp. 7884–7886, 2004.

[37] Y. Pan *et al.*, "Size-dependent cytotoxicity of gold nanoparticles," *Small*, vol. 3, no. 11, pp. 1941–1949, 2007.

[38] H. J. Yen, S. H. Hsu, and C. L. Tsai, "Cytotoxicity and immunological response of gold and silver nanoparticles of different sizes," *Small*, vol. 5, no. 13, pp. 1553–1561, 2009.

[39] S. Huo *et al.*, "Ultrasmall gold nanoparticles as carriers for nucleus-based gene therapy due to size-dependent nuclear entry," *ACS Nano*, vol. 8, no. 6, pp. 5852–5862, 2014.

[40] G. Li, D. Li, L. Zhang, J. Zhai, and E. Wang, "One-step synthesis of folic acid protected gold nanoparticles and their receptor-mediated intracellular uptake," *Chem. - A Eur. J.*, vol. 15, no. 38, pp. 9868–9873, 2009.

[41] Y. Lu and P. S. Low, "Folate-mediated delivery of macromolecular anticancer therapeutic agents," *Adv. Drug Deliv. Rev.*, vol. 64, no. SUPPL., pp. 342–352, 2012.

[42] P. Decuzzi and M. Ferrari, "The receptor-mediated endocytosis of nonspherical particles," *Biophys. J.*, vol. 94, no. 10, pp. 3790–3797, 2008.

[43] S. Nazir, T. Hussain, A. Ayub, U. Rashid, and A. J. MacRobert, "Nanomaterials in combating cancer: Therapeutic applications and developments," *Nanomedicine Nanotechnology, Biol. Med.*, vol. 10, no. 1, pp. 19–34, 2014.

[44] B. Khlebtsov, V. Zharov, A. Melnikov, V. Tuchin, and N. Khlebtsov, "Optical amplification of photothermal therapy with gold nanoparticles and nanoclusters," *Nanotechnology*, vol. 17, no. 20, pp. 5167–5179, 2006.

[45] S. K. Ghosh and T. Pal, "Interparticle Coupling Effect on the Surface Plasmon Resonance of Gold Nanoparticles: From Theory to Applications," *Chem. Rev.*, vol. 107, no. 11, pp. 4797–4862, 2007.

[46] H. Chen *et al.*, "Understanding the photothermal conversion efficiency of gold

View Article Online
DOI: 10.1039/D0TB00240B

nanocrystals," *Small*, vol. 6, no. 20, pp. 2272–2280, 2010.

[47] N. S. Abadeer and C. J. Murphy, "Recent Progress in Cancer Thermal Therapy Using Gold Nanoparticles," *J. Phys. Chem. C*, vol. 120, no. 9, pp. 4691–4716, 2016.

[48] L. Galluzzi *et al.*, "Molecular mechanisms of cell death: Recommendations of the Nomenclature Committee on Cell Death 2018," *Cell Death Differ.*, vol. 25, no. 3, pp. 486–541, 2018.

[49] H. H. Richardson, M. T. Carlson, P. J. Tandler, P. Hernandez, and A. O. Govorov, "Experimental and theoretical studies of light-to-heat conversion and collective heating effects in metal nanoparticle solutions," *Nano Lett.*, vol. 9, no. 3, pp. 1139–1146, 2009.

[50] X. Huang, W. Qian, I. H. El-Sayed, and M. A. El-Sayed, "The potential use of the enhanced nonlinear properties of gold nanospheres in photothermal cancer therapy," *Lasers Surg. Med.*, vol. 39, no. 9, pp. 747–753, 2007.

[51] S. Sabharanjak and S. Mayor, "Folate receptor endocytosis and trafficking," *Adv. Drug Deliv. Rev.*, vol. 56, no. 8, pp. 1099–1109, 2004.

[52] A. M. Pinilla, D. Blach, S. C. Mendez, and F. M. Ortega, "AOT direct and reverse micelles as a reaction media for anisotropic silver nanoparticles functionalized with folic acid as a photothermal agent on HeLa cells," *SN Appl. Sci.*, vol. 1, no. 8, 2019.

[53] R. Mendes, P. Pedrosa, J. C. Lima, A. R. Fernandes, and P. V. Baptista, "Photothermal enhancement of chemotherapy in breast cancer by visible irradiation of Gold Nanoparticles," *Sci. Rep.*, vol. 7, no. 1, pp. 1–9, 2017.

[54] A. Leonidova *et al.*, "Photo-induced uncaging of a specific Re(i) organometallic complex in living cells," *Chem. Sci.*, vol. 5, no. 10, pp. 4044–4056, 2014.

[55] A. L. Edinger and C. B. Thompson, "Death by design: Apoptosis, necrosis and autophagy," *Curr. Opin. Cell Biol.*, vol. 16, no. 6, pp. 663–669, 2004.

[56] J. D. Lane, V. J. Allan, and P. G. Woodman, "Active relocation of chromatin and endoplasmic reticulum into blebs in late apoptotic cells," *J. Cell Sci.*, vol. 118, no. 17, pp. 4059–4071, 2005.

[57] G. L. Zwicke, G. A. Mansoori, and C. J. Jeffery, "Targeting of Cancer Nanotherapeutics," *Nano Rev.*, vol. 1, pp. 1–11, 2012.

[58] N. C. L. Zembruski, V. Stache, W. E. Haefeli, and J. Weiss, "7-Aminoactinomycin D for apoptosis staining in flow cytometry," *Anal. Biochem.*, vol. 429, no. 1, pp. 79–81, 2012.

[59] O. Kepp, L. Galluzzi, M. Lipinski, J. Yuan, and G. Kroemer, "Cell death assays for drug discovery," *Nat. Rev. Drug Discov.*, vol. 10, no. 3, pp. 221–237, 2011.

[60] S. J. Martin, C. M. Henry, and S. P. Cullen, "A Perspective on Mammalian Caspases as Positive and Negative Regulators of Inflammation," *Mol. Cell*, vol. 46, no. 4, pp. 387–397, 2012.

[61] W. S. Kuo *et al.*, "Induction of ROS, mitochondrial damage and autophagy in lung epithelial cancer cells by iron oxide nanoparticles," *Biomaterials*, vol. 33, no. 20, pp. 2246–2249, 2012.

View Article Online
DOI: 10.1039/D0TB00240B

[62] A. Chompoosor *et al.*, "The role of surface functionality on acute cytotoxicity, ROS generation and DNA damage by cationic gold nanoparticles," *Small*, vol. 6, no. 20, pp. 2246–2249, 2010.

[63] S. G. Rhee, "H2O2, a necessary evil for cell signaling," *Science (80-.).*, vol. 312, no. 5782, pp. 1882–1883, 2006.

[64] S. Fink, B. C.-I. and immunity, and undefined 2005, "Apoptosis, pyroptosis, and necrosis: mechanistic description of dead and dying eukaryotic cells," *Am Soc Microbiol.*

[65] S. W. Ryter *et al.*, "Mechanisms of Cell Death in Oxidative Stress," *Antioxid. Redox Signal.*, vol. 9, no. 1, pp. 49–89, Jan. 2007.

[66] J. R. Melamed, R. S. Edelstein, and E. S. Day, "Elucidating the fundamental mechanisms of cell death triggered by photothermal therapy," *ACS Nano*, vol. 9, no. 1, pp. 6–11, 2015.

View Article Online
DOI: 10.1039/D0TB00240B

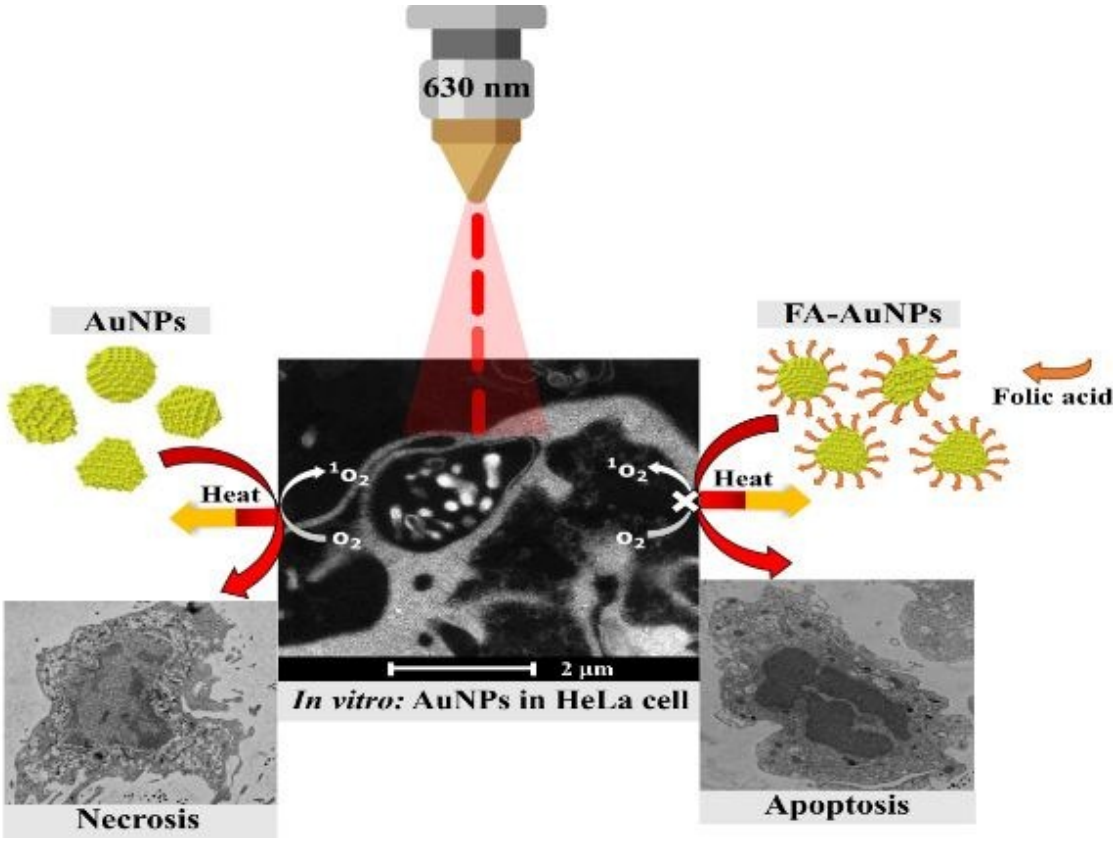

Schematic diagram exhibits the HeLa cell death during PPT treatment using folic acid conjugate gold nanoparticles FA-AuNPs and non-conjugated AuNPs.